Effect of ultrasound on the properties of rice bran protein and its chlorogenic acid complex

Tong Wang [a], Xing Chen [a], Weining Wang [b], Liqi Wang [b], Lianzhou Jiang [a], Dianyu Yu [a,*], Fengying Xie [a,*]

[a] School of Food Science, Northeast Agricultural University, Harbin 150030, China
[b] School of Computer and Information Engineering, Harbin University of Commerce, Harbin 150028, China

ARTICLE INFO

ABSTRACT

Ultrasound technology was used to treat rice bran protein (RBP), and the structural and functional properties of ultrasonically treated RBP (URBP) and its chlorogenic acid (CA) complex were studied. When ultrasonic power of 200 W was applied for 10 min, the maximum emission peak λ_{max} of the URBP-CA complex in the fluorescence spectrum was red-shifted by 3.6 nm compared to that of the untreated complex. The atomic force microscope (AFM) analysis indicated that the surface roughness of the complex was minimized (3.89 nm) at the ultrasonic power of 200 W and treatment time of 10 min. Under these conditions, the surface hydrophobicity (H_0) was 1730, the contents of the α-helix and β-sheet in the complex were 2.97% and 6.17% lower than those in the untreated sample, respectively, the particle size decreased from 106 nm to 18.2 nm, and the absolute value of the zeta-potential increased by 11.0 mV. Therefore, ultrasonic treatment and the addition of CA changed the structural and functional properties of RBP. Moreover, when ultrasonic power of 200 W was applied for 10 min, the solubility, emulsifying activity index (EAI), and emulsion stability index (ESI) were 68%, 126 m^2/g, and 37 min, respectively.

1. Introduction

Rice bran, with a protein content of approximately 15% [1], is the main by-product of rice processing [2]. Rice bran protein (RBP) is the main nutrient component in rice bran [3]. RBP is easy to digest and absorb in the body [4] and exhibits low allergenicity [5,6], which renders it highly suitable for infants, the elderly, and individuals with allergies [7,8]. Therefore, RBP is a desirable alternative for people with sensitive physique. Rafe et al. [9] mixed RBP with whey protein concentrate (WPC) to prepare a WPC-RBP mixed gel, which could be used as a functional food for infants and/or adults. However, RBP is mainly extracted from rice bran meal through alkali-soluble acid precipitation. This traditional process can lead to solubility and foaming, and the other functional and antioxidant properties of the extracted RBP may be deteriorated to a certain extent.

Ultrasound treatment is an emerging technology, and its application in the food industry has attracted widespread attention [10,11]. Ultrasonic modification is based on the principle that ultrasonic waves can generate mechanical vibrations between particles in the medium. Such vibrations release a certain amount of energy, which can trigger the interaction of medium particles to produce thermal, cavitation, and mechanical effects [12]. The cavitation effect, as a key aspect of ultrasound, produces strong micro jet and shear forces [13]. Ultrasonic technology has been widely used to modify the protein structure and functional properties. Gülseren et al. [14] studied the changes in protein structure after high-intensity ultrasonic treatment and noted that ultrasonic treatment could induce changes in the free sulfhydryl groups, particle size, surface hydrophobicity, and protein secondary structure. Albano et al. indicated that ultrasound treatment decreased the size of whey protein concentrate-pectin complexes and improved their functional properties [15]. Moreover, Marcuzzo et al. confirmed that ultrasonic treatment reduced protein aggregation and enhanced the uniformity of gluten-based films [16].

As the main antioxidant in food [17], polyphenols can interact with proteins, thereby affecting the structure, function, and nutritional properties of proteins, as well as the stability and bioavailability of polyphenols [18,19]. The essence of the interaction between polyphenols and proteins is the penetration of polyphenols into protein

---

molecules, and the two entities can be combined through covalent and non-covalent interactions. Non-covalent interactions mainly include hydrogen bonding, electrostatic adsorption, and hydrophobic interaction [20]. Chlorogenic acid (CA) is a common active phenolic acid found in coffee beans and citrus fruits. CA exhibits anti-oxidation capabilities, can inhibit obesity, and enable the treatment of the metabolic syndrome [21–23]. Zhang et al. [24] studied the non-covalent binding of CA with three kinds of whey proteins. The authors screened and obtained the most stable complex to prepare the CA-protein complex. Liu et al. [25] assessed the binding properties of CA with five milk proteins and highlighted that the van der Waals forces and hydrogen bond interactions were predominant between CA and α-casein and between CA and α-lactalbumin, respectively. Hydrophobic interactions were dominant between other complexes. However, the existing research on the properties of the complex of RBP and CA remains limited.

In this study, ultrasonic technology was used to treat RBP, and ultrasonically treated rice bran protein (URBP) was non-covalently combined with CA to prepare the URBP-CA complex. The effects of the treatment time and ultrasonic power on the structure and functional properties of the RBP and complex were examined. The objective was to enhance the functional properties of RBP and its complex and broaden the application range of RBP and its emulsion, thereby promoting the application of the URBP-CA complex in hypoallergenic products.

2. Materials and methods

2.1. Materials

Low-temperature defatted rice bran powder was purchased from Heilongjiang Beidahuang Agriculture Co., Ltd. (Harbin, China). Chlorogenic acid was purchased from Sinopharm Group Chemical Reagent Co., Ltd. (Shanghai, China). Soybean oil was purchased from Jiu San Grain and Oil Industry Group Co., Ltd. (Harbin, China). All other chemicals were commercially available and of analytical grade.

2.2. Extraction of RBP

Defatted rice bran was mixed with deionized water at a ratio of 1:10, and the pH was adjusted to 8.5 by using 2 mol/L NaOH solution. The mixture was stirred at 45 °C for 2 h and centrifuged at $5500 \times g$ for 15 min. The supernatant was extracted for subsequent steps. Next, 2 mol/L HCl solution was added to the supernatant to adjust the pH to 4.5, and the solution was centrifuged at $4500 \times g$ for 10 min to obtain a precipitate. The precipitate was washed three times using deionized water and centrifuged at $5000 \times g$ for 10 min. Subsequently, the pH was adjusted to 7.0 by using NaOH solution. The sample was freeze-dried to obtain the RBP with a protein content of 89.53%.

2.3. Ultrasonic treatment of RBP and preparation of URBP-CA complex

2.3.1. Ultrasonic treatment of RBP

A certain amount of RBP was dissolved in deionized water, and the pH was adjusted to 9.0 by using 2 mol/L NaOH solution. The RBP solutions were placed in a large beaker with ice to maintain the temperature at <20 °C, and the ultrasonic treatments were implemented using a Scientz-II D ultrasound generator (Scientz Biotechnology Co., Ltd., Ningbo, China). The titanium probe with a diameter of 6 mm was immersed in the solutions at a depth of 1 cm from the bottom, followed by treatment with ultrasound at 20 kHz for 10 and 20 min with ultrasonic power at 100 W and 200 W, respectively. After centrifugation at $4500 \times g$ for 10 min and freeze-dried treatment, the URBP was obtained.

2.3.2. Preparation of URBP-CA complex

The URBP was separately dissolved in phosphate buffer and prepared into a solution with a concentration of 1 g/100 mL. Subsequently, 0.1 g/100 mL CA was added to the solution. The mixture was stirred for 2 h at

25 °C and pH 7.4, centrifuged at $4500 \times g$ for 10 min, and freeze-dried to obtain URBP-CA complexes via treatment with ultrasonic power at 100 W and 200 W for 10 and 20 min, respectively. The process of ultrasonic treatment of RBP and preparation of URBP-CA complex is shown in Fig. 1.

2.4. Structural properties of URBP and URBP-CA complex

2.4.1. Analysis of fluorescence spectra

The prepared sample was added to deionized water to prepare a complex solution with a concentration of 0.1 g/100 mL. The parameter settings for the fluorescence spectrum measurement were as follows: The excitation wavelength was 280 nm, fluorescence excitation slit and emission slit wavelengths were 5 nm and 10 nm, respectively, and optical path of the quartz sample cell was 0.4 cm. Fluorescence in the range of 300–400 nm was analyzed.

2.4.2. Atomic force microscopy (AFM) analysis

The sample was scanned in the "tap" mode, and the height of the probe resonance fluctuation was recorded according to the fluctuation of the sample surface. The change in the height was controlled to obtain the sample surface morphology. The sample with a concentration of 10 ppm was smeared on the surface of the mica sheet and dried in air overnight. The dried samples were collected at room temperature with a driving frequency of 320 kHz and scanning frequency of 1.0 Hz, respectively. AFM images were collected with a scanning area of 2×2 μm. NanoScope Analysis 1.5 (Veeco, USA) was used to analyze the image and data.

2.4.3. Analysis of surface hydrophobicity (H_0)

H_0 was measured according to the method proposed by Kato & Nakai [26]. Specifically, 0.01 mol/L phosphate buffer (pH 7.4) was added to the sample to prepare a solution with a concentration range of 0.05–0.4 mg/mL. Subsequently, 4.0 mL of the solution was extracted and added to 20 μL of 10.0 mmol/L 8-anilino-1-naphthalenesulfonic acid (ANS). After mixing, the fluorescence intensities of the protein, complex solution, and phosphate buffer solution (blank sample) were determined. The fluorescence settings were as follows: The excitation wavelength was 390 nm, emission wavelength was 468 nm, and slit width was 5 nm.

2.4.4. Analysis of Fourier transform infrared (FTIR) spectroscopy

One milligram of sample was extracted, and 100 mg of KBr was added to it. Next, the sample was evaluated using an 8400S Fourier infrared spectrometer. The scanning range was 500–4000 cm^{-1}, and the resolution was 4 cm^{-1}. The content distribution of each secondary structure of the protein was obtained using the Peakfit 4.12 software [27].

2.4.5. Analysis of the particle size and zeta-potential

A Zetasizer Nano ZS potential and particle size distribution meter was used to determine the particle size distribution and zeta-potential of the sample. The sample solution was diluted with 0.01 M phosphate buffer (pH 7.0) as a dispersant. The particle and dispersant refractive indices were set as 1.46 and 1.33, respectively. The particle size distribution was measured at 25 °C, and the zeta-potential of the sample was simultaneously measured.

2.5. Functional properties of URBP and URBP-CA complex

2.5.1. Analysis of solubility

Ten milliliters of sample solution with a concentration of 100 μg/mL was centrifuged at $3000 \times g$ for 15 min. The protein content in the supernatant was determined according to Lowry's method [28]. A standard curve was drawn using bovine serum albumin as the standard substance, and the total protein content of the sample solution was determined according to the Kjeldahl method. The solubility of the
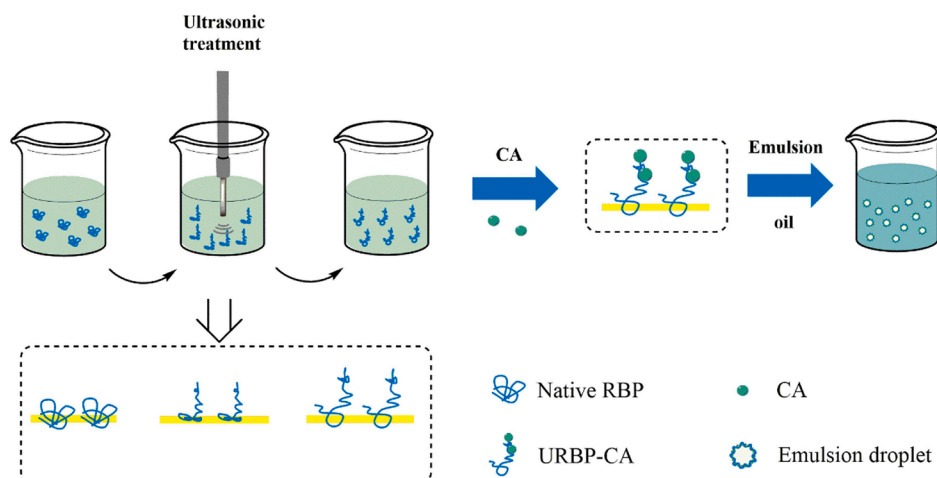
Fig. 1. Schematic of ultrasonic mechanism of RBP and URBP-CA complex.

samples was calculated as follows:

$$Solubility(\%) = \frac{Concentration\ of\ protein\ in\ supernatant}{Concentration\ of\ total\ protein} \times 100 \qquad (1)$$

2.5.2. Analysis of emulsification properties

Nine milliliters of the sample solution was obtained. Subsequently, 3 mL of soybean oil was added to the solution [29]. The sample was homogenized (Ultra-Turrax T18, Angni Co., Ltd., Shanghai, China) at 10,000 rpm for 3 min. The emulsion was further homogenized in a high-pressure homogenizer (FPG12805, Standard Fluid Power Ltd., England, UK) at 80 MPa for two cycles. Next, 50 μL of the sample was pipetted at the bottom and diluted with 0.1% (w/v) sodium dodecyl sulfate solution. The absorbance value A_0 of the sample solution and absorbance value A_{10} after retaining the mixture for 10 min were measured at a wavelength of 500 nm. The emulsifying activity index (EAI) and emulsion stability index (ESI) were calculated as follows:

$$EAI\left(m^2/g\right) = 2 \times 2.303 \frac{A_0 \times N}{C \times \varphi \times 10000} \qquad (2)$$

$$ESI(min) = \frac{A_0}{A_0 - A_{10}} \times (T_{10} - T_0) \qquad (3)$$

where N represents the dilution factor, C represents the sample concentration (g/100 mL), Φ represents the volume fraction of oil phase in the composite emulsion, A_0 and A_{10} represent the absorbance values at 0 min and 10 min, respectively, and T_{10}-T_0 is the time difference, which is 10 min.

2.6. Statistical analysis

All the measurements were conducted at least in triplicate, and the mean value and standard deviations were analyzed. Origin 9.0 and Peakfit 4.12 were used to analyze the data. Statistics17 was used to analyze the variance, and Duncan's test (p < 0.05) was used to evaluate the significance of the data differences.

3. Results and discussion

3.1. Effect of ultrasonic treatment of RBP on the structural properties of URBP and URBP-CA complex

3.1.1. Fluorescence spectrum analysis of URBP and URBP-CA complex

The endogenous fluorescence was considered to analyze the changes in the RBP and complex structure in different ultrasonic conditions. In general, at a wavelength of 280 nm, the main chromophores in the

fluorescence spectrum of the samples are tryptophan and tyrosine. These two groups are often considered to analyze the interaction between the proteins and various small molecules [30]. Fig. 2 shows that the fluorescence intensity of untreated RBP was higher than that of URBP, and this phenomenon also occurred in the URBP-CA complex. This indicates that the structure of the RBP was changed to a certain extent owing to the ultrasonic treatment. Compared with that of the untreated RBP, λ_{max} of URBPs exhibited different degrees of red-shift. The red-shift was the most notable (3.6 nm) when the ultrasonic conditions were 200 W and 10 min (Fig. 2a). This was because ultrasonic treatment unfolded the structure of the protein, the originally buried aromatic amino acid residues were exposed to the surface of the protein, and the polarity of the microenvironment increased [31,32]. When CA was added to form a complex, the λ_{max} of the complex was red-shifted compared with that before complexing. The red-shift of λ_{max} could be attributed to the formation of intermolecular hydrogen bonds between the hydroxyl groups of CA and sulfhydryl groups or hydroxyl groups of the protein [33]. In addition, as the ultrasound time increased, the fluorescence intensity of the URBP and its complexes significantly decreased. The phenomenon occurred because the formation and collapse of bubbles during ultrasonic treatment led to cavitation effects, which increased the shear force. Consequently, the protein structure was fully unfolded, and more hydrophobic groups were exposed to the surface of the protein molecules. The hydrophobic interaction between the molecules was promoted, the protein formed aggregates, and the exposed aromatic amino acids were buried again, resulting in a decreased fluorescence intensity.

3.1.2. AFM analysis of URBP and URBP-CA complex

AFM is a powerful analysis method to clarify the surface morphology and particle size distribution of proteins and complexes. As shown in Fig. 3, the radius and height of the RBP and complexes after ultrasonic treatment were reduced, and the surface roughness (Rq) of the untreated RBP was 15.4 nm. Ultrasound treatment can unfold the spatial structure of the protein and turn the protein, which was originally in a disorderly aggregate state, into more regular and dispersed aggregates [34]. The addition of CA facilitated the hydrophobic interaction of the complex and formation of intermolecular hydrogen bonds, leading to the formation of more dispersed soluble aggregates. The minimum Rq of the complex was 3.89 nm at 200 W for 10 min. When the ultrasound time and power were high, the soluble aggregates continued to aggregate, and the size of the protein particles increased, resulting in an increase in the radius and height of the soluble aggregates as well as an increase in Rq.

3.1.3. H_0 analysis of URBP and URBP-CA complex

H_0 is usually used to clarify changes in the protein conformation
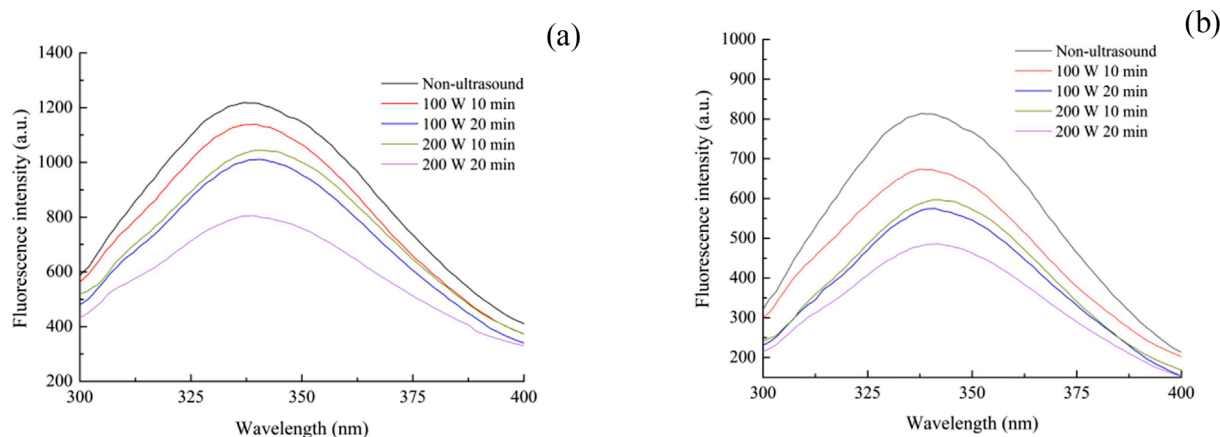
Fig. 2. Fluorescence spectra of URBP (a) and URBP-CA complex (b) under different ultrasonic conditions.

before and after sample processing. Notably, the distribution of hydrophobic residues on the protein surface is usually characterized by H_0. As shown in Fig. 4, the addition of CA caused the H_0 of the complex to exhibit a downward trend compared with the untreated RBP. This phenomenon occurred because the introduction of CA caused a certain aggregation of exposed groups under hydrophobic action. The formed aggregates had a shielding effect on the hydrophobic region of RBP, reduced the binding degree of the hydrophobic groups to the fluorescent probe ANS, and led to a decrease in H_0. Moreover, after ultrasonic treatment, the H_0 value of the complex significantly increased. With the increase in the ultrasonic power, the H_0 value exhibited a rising trend. This might be due to the gradual unfolding of the RBP structure after ultrasonic treatment, which promoted the exposure of more hydrophobic groups [35], causing the H_0 of the solution to increase. However, with the increase in the ultrasonic time, the unfolded structure aggregated, and the binding degree between the hydrophobic groups and fluorescent probe ANS reduced, resulting in a decrease in H_0 [36].

3.1.4. FTIR analysis of URBP and URBP-CA complex

FTIR spectroscopy is an optical detection method for analyzing the secondary structure of protein. The absorption peak of the protein amide I band in the RBP and RBP-CA complex ranges from 1700 to 1600 cm^{-1}, which is the most commonly used band to reflect the changes in the protein secondary structure [37]. The changes in the FTIR spectra of RBP and complex under different conditions are shown in Fig. 5.

According to existing studies, the wave number ranges 1646–1664 cm^{-1} corresponding to an α-helix structure. The wave number ranges 1615–1637 cm^{-1} and 1682–1700 cm^{-1} corresponding to a β-sheet structure. The wave number ranges 1664–1681 cm^{-1} and 1637–1645 cm^{-1} corresponding to β-turn and random coil structures, respectively [38]. The Gaussian integration method is used to fit and calculate the content of each secondary structure. The results of the secondary structure content of RBP and complex under different conditions are presented in Table 1. After the addition of the CA, the α-helix content of the complex decreased from 22.62% to 21.81%; β-sheet content decreased from 41.01% to 39.43%; β-turn content increased significantly (p < 0.05), from 17.39% to 18.45%; and random coil content increased from 18.98% to 20.31%. These trends can be explained by the formation of hydrogen bonds and hydrophobic interaction between the CA and RBP, resulting in the rearrangement of the peptide chain of the RBP and modification of the secondary structure of the RBP, which can prove the interaction between the RBP and CA.

Moreover, in different ultrasonic conditions, the α-helix content and β-sheet content of the complex decreased, and the β-turn and random coil content increased. The α-helix and β-sheet structures gradually changed to β-turn and random coil structures. This is because, in general, the secondary structure of protein mainly depends on the sequence

of amino acids and hydrogen bonds. In the ultrasonic treatment, the formation and collapse of bubbles led to cavitation effects, which increased the physical forces such as turbulence and shear force. Moreover, ultrasonic treatment changed the arrangement of hydrogen bonds in the RBP molecules, resulting in several α-helix structures converting to β-turn and random coil structures [39]. Therefore, the α-helix content decreased and the β-turn and random coil contents increased. However, with the increase in the ultrasonic time, a considerable amount of heat and oxidation was generated, which promoted the aggregation of the RBP. Therefore, the content of the α-helix and β-sheet structures increased, and the content of the β-turn and random coil structures decreased. This result is consistent with Xia et al.'s research regarding the secondary structure of soy protein isolate at different ultrasound periods [40].

3.1.5. Analysis of particle size and zeta-potential of URBP and URBP-CA complex

The particle size of a protein is often used to characterize the degree of aggregation of the protein, which influences the solubility and other functional properties of the protein [41]. Fig. 6 shows that the particle size of the RBP and complex solution without ultrasonic treatment exhibited a bimodal distribution. The particle size distribution of the pure RBP solution was narrower than that of the complex solution, and the particle size was smaller. The hydroxyl groups on the surface of the CA bound to the RBP through non-covalent interactions, thereby reducing the surface hydrophobicity and increasing the particle size of the complex. During the ultrasonic treatment, physical forces such as the turbulence and shear generated by cavitation destroyed the spatial structure of the protein. This phenomenon induced collisions between the proteins and reduced the particle size. The particle size distribution range of the URBP-CA complex solution at 200 W for 10 min was relatively narrow and the particle size was small. However, as the ultrasound time increased, the average particle size of the protein and complex particles increased, which indicated that the protein formed uneven aggregates after a long period of treatment.

The zeta-potential can reflect the stability of the solution system. Changes in the zeta-potential of the RBP and complex in different conditions are shown in Fig. 7. The absolute value of the zeta-potential of the untreated RBP and complex was the lowest. The zeta-potential of the URBP increased with the increase in the ultrasonic power. When the ultrasonic power was 200 W, the absolute value of the zeta-potential was relatively high. This phenomenon occurred because under the action of the ultrasound, the originally dense structure of the RBP unfolded, the polar groups originally buried inside were exposed to the surface of the protein particles, and the exposed charge increased. Under the same ultrasonic treatment conditions, the absolute value of the complex potential was slightly lower than that of the RBP, likely because the
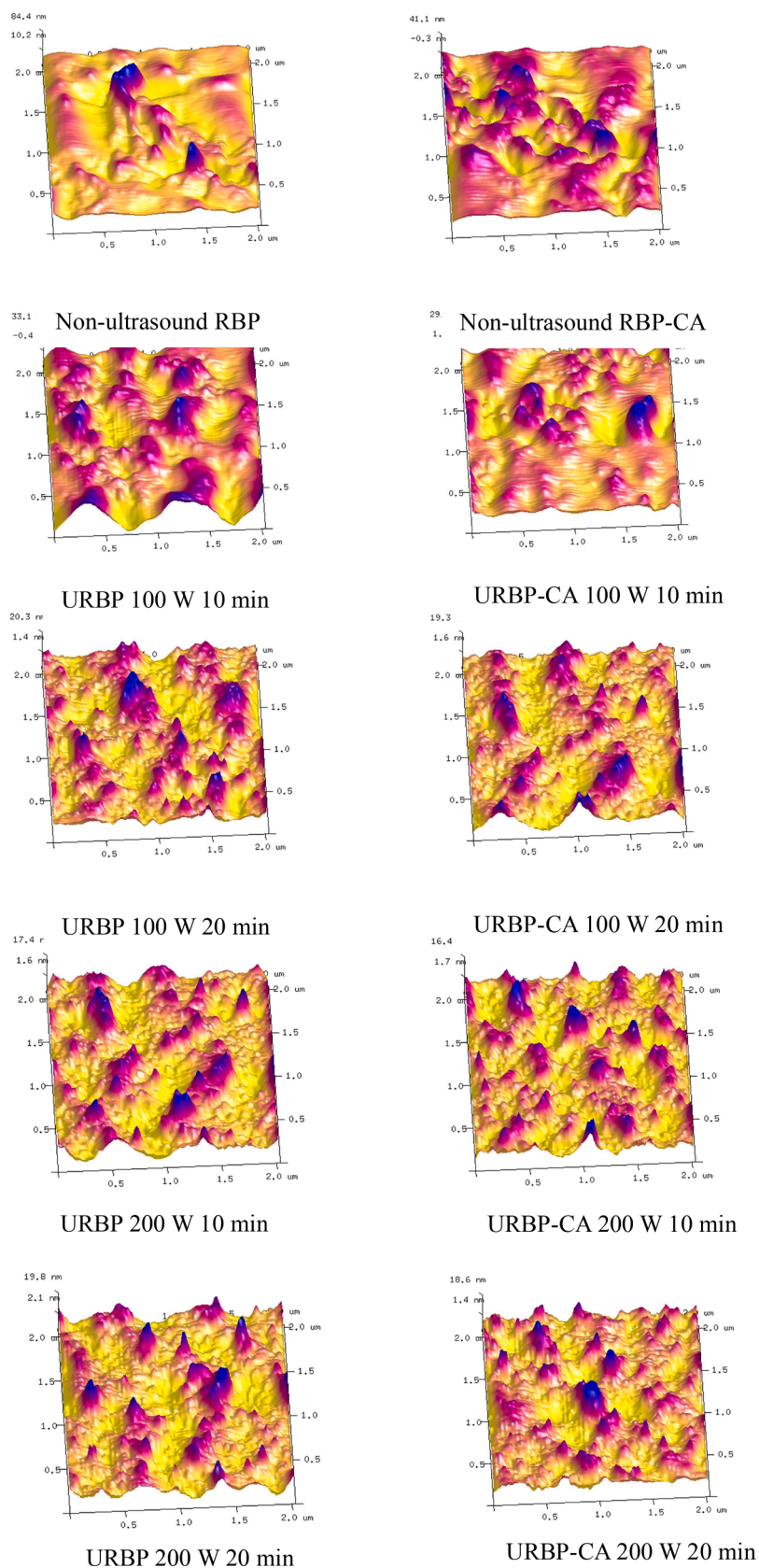
Non-ultrasound RBP

Non-ultrasound RBP-CA

URBP 100 W 10 min

URBP-CA 100 W 10 min

URBP 100 W 20 min

URBP-CA 100 W 20 min

URBP 200 W 10 min

URBP-CA 200 W 10 min

URBP 200 W 20 min

URBP-CA 200 W 20 min

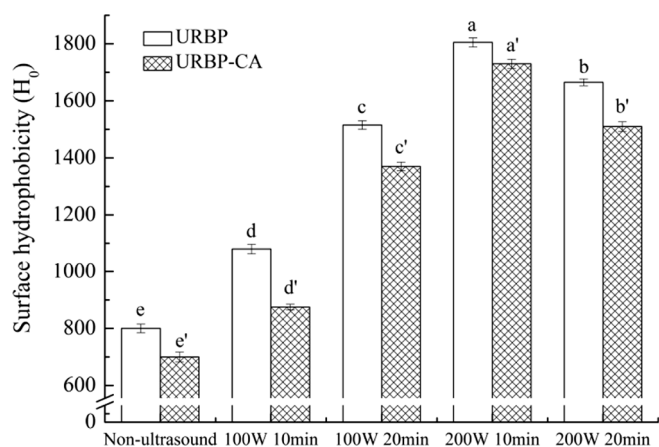**Fig. 3.** AFM images of URBP and URBP-CA complex under different ultrasonic conditions.

Fig. 4. Surface hydrophobicity analysis of URBP and URBP-CA complex under different ultrasonic conditions. Note: The superscript letters in the same group indicate significant differences among the data (p < 0 0.05).

ultrasonic treatment exposed the internal structure of the protein molecule and increased the contact between the inner protein and CA. A large number of CA molecules were observed to be in the solution, and electrostatic interaction occurred between the carboxyl groups on CA and cationic region of the protein [42], which reduced the absolute value of the complex solution potential. When the ultrasonic power was 200 W, a higher treatment time caused the protein to aggregate to a certain extent, which masked the polar sites on the surface of the protein, resulting in a reduction in the absolute value of the zeta-potential.

3.2. Effect of ultrasonic treatment of RBP on the functional properties of URBP and URBP-CA complex

3.2.1. Solubility analysis of the URBP and URBP-CA complex

The solubility of protein in food components is closely related to its emulsifying and gelling properties. The changes in the solubility of the RBP and complexes under different conditions are shown in Fig. 8. Compared with pure RBP, the solubility was reduced after the addition of CA. The addition of CA facilitated the hydrophobic interaction of the complex, which led to a reduced solubility. The solubility of URBP was higher than that of RBP without ultrasonic treatment. As the ultrasonic power increased, the solubility of the complex significantly increased. The solubility of URBP and the complex were the largest when the ultrasonic power was 200 W and treatment time was 10 min. It is likely that the strong physical force generated by the ultrasonic cavitation destroyed the non-covalent bonds (electrostatic interaction,

hydrophobic interaction, etc.) that maintained the protein spatial structure and promoted the unfolding of the RBP structure. Furthermore, the hydrophobic and polar groups inside the protein molecule were exposed to the surface, increasing the interaction between the protein particles and water [43], thereby improving the solubility of the RBP. Notably, long-term ultrasonic treatment caused the unfolded protein structure to re-aggregate, which modified the solubility of the protein in water [44]. This result is consistent with those of the particle size.

3.2.2. Analysis of emulsification properties of URBP and URBP-CA complex solution

Emulsification properties are key properties of the RBP. EAI and ESI can be used as indicators of the emulsification properties. The EAI of protein can reflect the ability of the complex to form an emulsified layer at the oil–water interface [45]. Fig. 9 shows that the EAI of the complex was significantly higher than that of the RBP, indicating that the addition of CA can increase the binding of the protein at the oil–water interface, thereby enhancing the emulsification ability of the protein. Compared with the untreated RBP and complex, the EAI of URBP and

Table 1
Changes of secondary structure content of RBP and RBP-CA complex under different ultrasonic conditions.

Sample	α -helix (%)	β-sheet (%)	β-turn (%)	random coil (%)
Non-ultrasound RBP	22.62 ± 0.30[a]	41.01 ± 0.12[a]	17.39 ± 0.20 [h]	18.98 ± 0.12 [g]
Non-ultrasound RBP-CA	21.81 ± 0.08[b]	39.43 ± 0.11[c]	18.45 ± 0.12[f]	20.31 ± 0.10[e]
URBP 100 W 10 min	22.53 ± 0.15[a]	39.85 ± 0.12[b]	18.07 ± 0.12 [g]	19.55 ± 0.14[f]
URBP-CA 100 W 10 min	22.04 ± 0.11[b]	38.64 ± 0.18[d]	18.75 ± 0.13[e]	20.57 ± 0.19[d]
URBP 100 W 20 min	22.01 ± 0.12[b]	38.43 ± 0.12[d]	19.05 ± 0.13[d]	20.51 ± 0.17[de]
URBP-CA 100 W 20 min	21.05 ± 0.13[c]	37.37 ± 0.16[e]	18.59 ± 0.13[ef]	22.99 ± 0.15[b]
URBP 200 W 10 min	20.05 ± 0.15[e]	34.82 ± 0.12 [h]	22.84 ± 0.13[b]	22.29 ± 0.11[c]
URBP-CA 200 W 10 min	18.84 ± 0.19[f]	33.26 ± 0.13[i]	24.88 ± 0.11[a]	23.02 ± 0.11[b]
URBP 200 W 20 min	21.83 ± 0.11[b]	36.02 ± 0.11[f]	18.68 ± 0.11[ef]	23.47 ± 0.13[a]
URBP-CA 200 W 20 min	20.64 ± 0.12[d]	35.45 ± 0.10 [g]	20.72 ± 0.16[c]	23.19 ± 0.10[b]

Note: The different superscript letters in the same column indicate significant differences between data (p < 0.05).
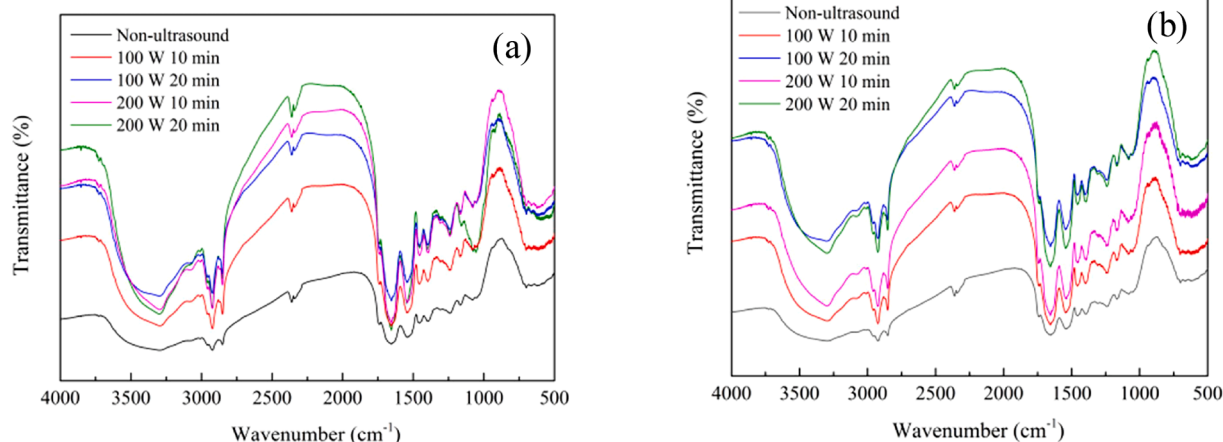

Fig. 5. FTIR analysis of URBP (a) and URBP-CA complex (b) under different ultrasonic conditions.
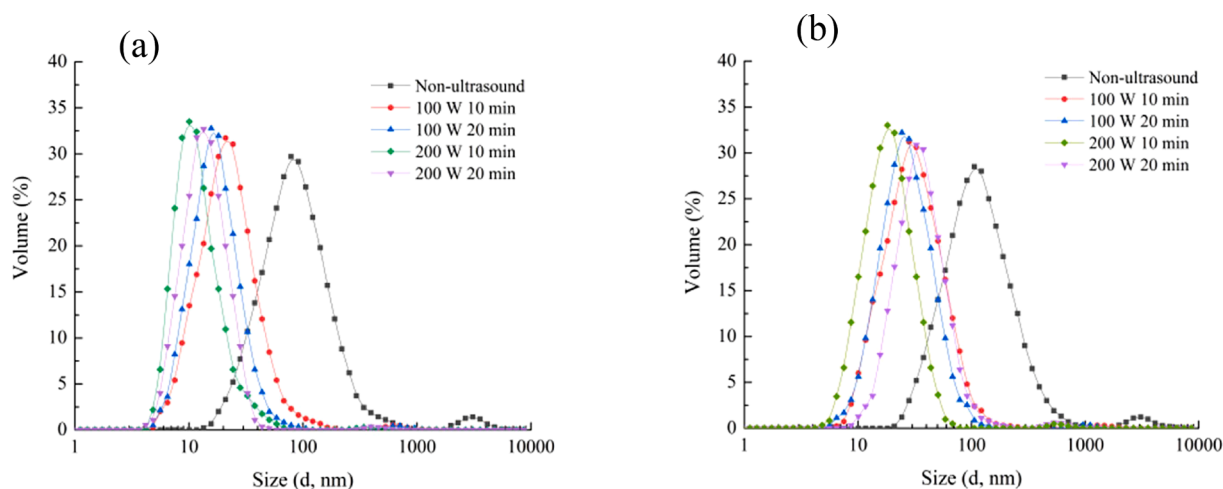
Fig. 6. Particle size of URBP (a) and URBP-CA complex (b) under different ultrasonic conditions.
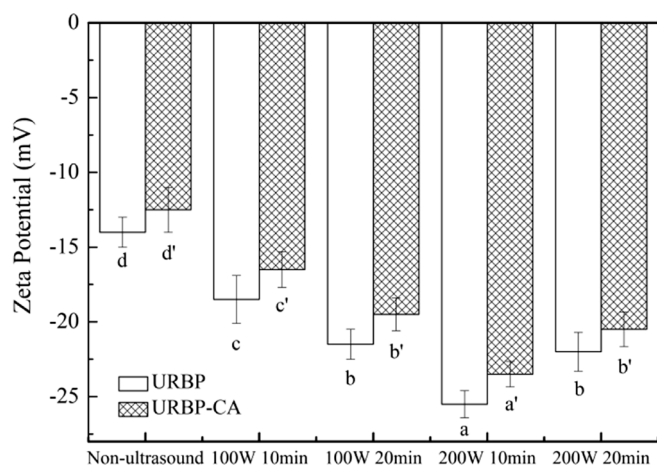

Fig. 7. Zeta-potential of URBP and URBP-CA complex under different ultrasonic conditions. Note: The superscript letters in the same group indicate significant differences among the data ($p < 0.05$).
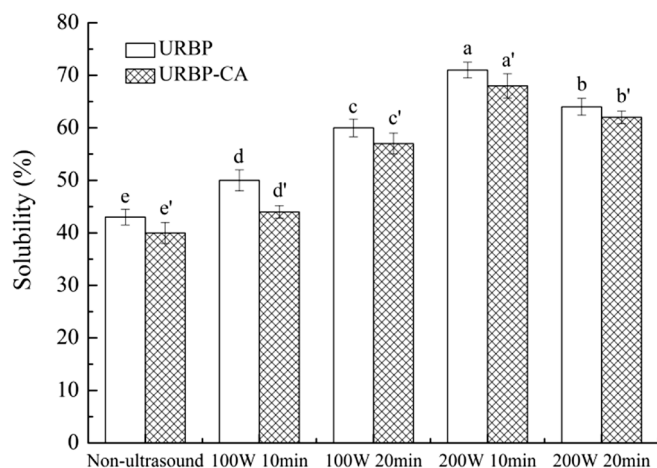

Fig. 9. EAI of URBP and URBP-CA complex solution under different ultrasonic conditions. Note: The superscript letters in the same group indicate significant differences among the data ($p < 0.05$).
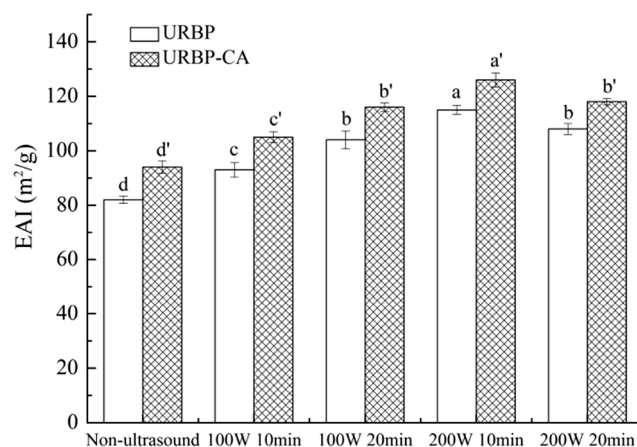

Fig. 8. Solubility of URBP and URBP-CA complex under different ultrasonic conditions. Note: The superscript letters in the same group indicate significant differences among the data ($p < 0.05$).

complex was significantly higher, and the EAI was high when the ultrasonic condition was 200 W for 10 min. After ultrasonic treatment, the structure of the RBP unfolded; consequently, its hydrophobic groups extended into the oil phase, and the hydrophilic group extended into the water phase to form a liquid film that could stabilize the oil droplets and increase the EAI. However, when the time was excessively high, part of the RBP denatured, the solubility decreased, and the EAI decreased.

The ESI reflects the stability of the emulsion formed by the protein and complex. The changes in the ESI of RBP and complex under different conditions are shown in Fig. 10. The trend of the ESI of RBP is consistent with that of the EAI. The ESI of the RBP and complex after ultrasonic treatment were significantly higher than those of the untreated samples, and the ESI of the complex was higher than that of the RBP at the ultrasonic conditions of 200 W for 10 min. The ultrasonic treatment unfolded the protein structure and strengthened the affinity of the oil–water interface [46], thereby enhancing the ESI. However, an excessively high ultrasound time affected the distribution of the proteins and complexes at the oil–water interface and caused conformational rearrangement, resulting in a decrease in the ESI. The addition of the CA promoted the hydrophobic interaction of the URBP-CA complex, which enhanced the adsorption of protein onto the oil–water interface and increased the ESI of the complex [24,47]. Overall, the structure and functional properties of the URBP-CA complex are superior when an ultrasonic power of 200 W was applied for 10 min.
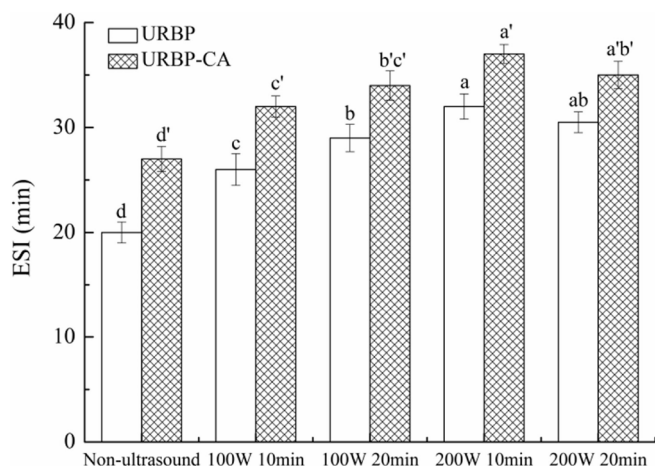
Fig. 10. ESI of URBP and URBP-CA complex solution under different ultrasonic conditions. Note: The different superscript letters in the same group indicate significant differences between data (p < 0.05).

4. Conclusions

The structure of the RBP was modified by ultrasonic treatment and the resulting protein was combined with CA via non-covalent interactions to form URBP-CA complexes. After ultrasonic treatment, the fluorescence intensity of the RBP decreased, and λ_{max} exhibited a certain degree of red-shift. After the addition of CA, the performance enhanced. According to the AFM results, the radius and height of the RBP and complex treated with ultrasound were reduced, as well as the Rq value. The analysis of the secondary structure content of the URBP and URBP-CA complexes demonstrated that the content of the α-helix and β-sheet structures decreased, and the content of the β-turn and random coil increased. Under the ultrasonic conditions of 200 W and 10 min, the URBP-CA complex exhibited a superior surface hydrophobicity, smaller particle size, and larger absolute value of the zeta-potential. Moreover, the research regarding the functional properties of URBP and URBP-CA complex highlighted that the URBP-CA complex subjected to ultrasound treatment could effectively increase the solubility, EAI, and ESI of RBP. The findings can promote the application of the URBP-CA complex.

CRediT authorship contribution statement

Tong Wang: Methodology, Investigation, Writing – original draft. **Xing Chen:** Investigation, Validation, Data curation. **Weining Wang:** Data curation, Visualization. **Liqi Wang:** Supervision, Funding acquisition. **Lianzhou Jiang:** Supervision, Conceptualization. **Dianyu Yu:** Conceptualization, Methodology, Writing - review & editing. **Fengying Xie:** Supervision, Conceptualization.

Declaration of Competing Interest

The authors declare that they have no known competing financial interests or personal relationships that could have appeared to influence the work reported in this paper.

Acknowledgements

References:

[1] J.S. Hamada, Characterization and Functional Properties of Rice Bran Proteins Modified by Commercial Exoproteases and Endoproteases, J. Food Sci. 65 (2) (2000) 305–310, https://doi.org/10.1111/j.1365-2621.2000.tb15998.x.

[2] J. Choi, M. Jeon, W. Moon, J. Moon, E.J. Cheon, J. Kim, S.K. Jung, Y. Ji, S.W. Son, M. Kim, In Vivo Hair Growth-Promoting Effect of Rice Bran Extract Prepared by Supercritical Carbon Dioxide Fluid, Biol. Pharm. Bull. 37 (2014) 44–53, https://doi.org/10.1248/bpb.b13-00528.

[3] C. Fabian, Y.-H. Ju, A Review on Rice Bran Protein: Its Properties and Extraction Methods, Crit. Rev. Food Sci. Nutr. 51 (9) (2011) 816–827, https://doi.org/10.1080/10408398.2010.482678.

[4] S. Han, K. Chee, S. Cho, Nutritional quality of rice bran protein in comparison to animal and vegetable protein, Food Chem. 172 (2015) 766–769, https://doi.org/10.1016/j.foodchem.2014.09.127.

[5] T. Supriyati, T. Haryati, I.W.R. Susanti, Susana, Nutritional Value of Rice Bran Fermented by Bacillus amyloliquefaciens and Humic Substances and Its Utilization as a Feed Ingredient for Broiler Chickens, Asian Austral. J. Anim. 28 (2015) 231–238, https://doi.org/10.5713/ajas.14.0039.

[6] R. Satoh, I. Tsuge, R. Tokuda, R. Teshima, Analysis of the distribution of rice allergens in brown rice grains and of the allergenicity of products containing rice bran, Food Chem. 276 (2019) 761–767, https://doi.org/10.1016/j.foodchem.2018.10.080.

[7] I. Lima, H. Guraya, E. Champagne, The functional effectiveness of reprocessed rice bran as an ingredient in bakery products, Nahrung/Food 46 (2002) 112–117, https://doi.org/10.1002/1521-3803(20020301)46:2<112::AID-FOOD112>3.0.CO;2-N.

[8] M.K. Sharif, M.S. Butt, F.M. Anjum, S.H. Khan, Rice Bran: A Novel Functional Ingredient, Crit. Rev. Food Sci. Nutr. 54 (6) (2014) 807–816, https://doi.org/10.1080/10408398.2011.608586.

[9] A. Rafe, E. Vahedi, A.G. Hasan-Sarei, Rheology and microstructure of binary mixed gel of rice bran protein-whey: effect of heating rate and whey addition, J. Sci. Food Agric. 96 (11) (2016) 3890–3896, https://doi.org/10.1002/jsfa.7586.

[10] C. Arzeni, O.E. Pérez, A.M.R. Pilosof, Functionality of egg white proteins as affected by high intensity ultrasound, Food Hydrocolloid. 29 (2) (2012) 308–316, https://doi.org/10.1016/j.foodhyd.2012.03.009.

[11] J. Gu, Q. Li, J. Liu, Z. Ye, T. Feng, G. Wang, W. Wang, Y. Zhang, Ultrasonic–assisted extraction of polysaccharides from Auricularia auricula and effects of its acid hydrolysate on the biological function of Caenorhabditis elegans, Int. J. Biol. Macromol. 167 (2021) 423–433, https://doi.org/10.1016/j.ijbiomac.2020.11.160.

[12] K.H. Kampert, R. Albrecht, T.C. Awes, P. Beckmann, F. Berger, R. Bock, G. Claesson, G. Clewing, L. Dragon, A. Eklund, R.L. Ferguson, A. Franz, S. Garpman, R. Glasow, H.Å. Gustafsson, H.H. Gutbrod, G. Holker, J. Idh, P. Jacobs, B.W. Kolb, H. Löhner, I. Lund, F.E. Obenshain, A. Oskarsson, I. Otterlund, T. Peitzmann, F. Plasil, A.M. Poskanzer, M. Purschke, H.G. Ritter, S. Saini, R. Santo, H.R. Schmidt, S.P. Sørensen, K. Steffens, E. Stenlund, D. Stüken, G.R. Young, Bose-Einstein correlations in the target fragmentation region of 200 A GeV ^{16}O + nucleus collisions, Nucl. Phys. A 525 (1991) 333–337, https://doi.org/10.1016/0375-9474(91)90342-4.

[13] B. Khadhraoui, V. Ummat, B.K. Tiwari, A.S. Fabiano-Tixier, F. Chemat, Review of ultrasound combinations with hybrid and innovative techniques for extraction and processing of food and natural products, Ultrason. Sonochem. 76 (2021) 105625, https://doi.org/10.1016/j.ultsonch.2021.105625.

[14] İ. Gülseren, D. Güzey, B.D. Bruce, J. Weiss, Structural and functional changes in ultrasonicated bovine serum albumin solutions, Ultrason. Sonochem. 14 (2) (2007) 173–183, https://doi.org/10.1016/j.ultsonch.2005.07.006.

[15] K.M. Albano, V.R. Nicoletti, Ultrasound impact on whey protein concentrate-pectin complexes and in the O/W emulsions with low oil soybean content stabilization, Ultrason. Sonochem. 41 (2018) 562–571, https://doi.org/10.1016/j.ultsonch.2017.10.018.

[16] E. Marcuzzo, D. Peressini, F. Debeaufort, A. Sensidoni, Effect of ultrasound treatment on properties of gluten-based film, Innov. Food Sci. Emerg. 11 (3) (2010) 451–457, https://doi.org/10.1016/j.ifset.2010.03.002.

[17] F. Zhu, Polysaccharide based films and coatings for food packaging: Effect of added polyphenols, Food Chem. 359 (2021) 129871, https://doi.org/10.1016/j.foodchem.2021.129871.

[18] H.M. Rawel, D. Czajka, S. Rohn, J. Kroll, Interactions of different phenolic acids and flavonoids with soy proteins, Int. J. Biol. Macromol. 30 (3-4) (2002) 137–150, https://doi.org/10.1016/S0141-8130(02)00016-8.

[19] P.-J. Tsai, C.-H. She, Significance of Phenol−Protein Interactions in Modifying the Antioxidant Capacity of Peas, J. Agric. Food Chem. 54 (22) (2006) 8491–8494, https://doi.org/10.1021/jf061475y.

[20] K. Nagy, M.-C. Courtet-Compondu, G. Williamson, S. Rezzi, M. Kussmann, A. Rytz, Non-covalent binding of proteins to polyphenols correlates with their amino acid sequence, Food Chem. 132 (3) (2012) 1333–1339, https://doi.org/10.1016/j.foodchem.2011.11.113.

[21] I. Onakpoya, R. Terry, E. Ernst, The Use of Green Coffee Extract as a Weight Loss Supplement: A Systematic Review and Meta-Analysis of Randomised Clinical Trials, Gastroent. Res. Pract. 2011 (2011) 1–6, https://doi.org/10.1155/2011/382852.

[22] J. Santana-Gálvez, L. Cisneros-Zevallos, D. Jacobo-Velázquez, Chlorogenic Acid: Recent Advances on Its Dual Role as a Food Additive and a Nutraceutical against Metabolic Syndrome, Molecules 22 (2017) 358, https://doi.org/10.3390/molecules22030358.

[23] P. Yin, S. Xie, Z. Zhuang, H. Fang, L. Tian, Y. Liu, J. Niu, Chlorogenic acid improves health in juvenile largemouth bass (Micropterus salmoides) fed high-fat diets:

Involvement of lipid metabolism, antioxidant ability, inflammatory response, and intestinal integrity, Aquaculture 545 (2021) 737169, https://doi.org/10.1016/j.aquaculture.2021.737169.

[24] Y. Zhang, Y. Lu, Y. Yang, S. Li, C.e. Wang, C. Wang, T. Zhang, Comparison of non-covalent binding interactions between three whey proteins and chlorogenic acid: Spectroscopic analysis and molecular docking, Food Biosci. 41 (2021) 101035, https://doi.org/10.1016/j.fbio.2021.101035.

[25] J. Liu, Q. Wang, H. Zhang, D. Yu, S. Jin, F. Ren, Interaction of chlorogenic acid with milk proteins analyzed by spectroscopic and modeling methods, Spectrosc. Lett. 49 (1) (2016) 44–50, https://doi.org/10.1080/00387010.2015.1066826.

[26] A. Kato, S. Nakai, Hydrophobicity Determination by a Fluorescence Probe Method and its Correlation with Surface Properties of Proteins, Biochim. Biophys. Acta 624 (1980) 13–20, https://doi.org/10.1016/0005-2795(80)90220-2.

[27] D. Yu, Y. Zhao, T. Li, D. Li, S. Chen, N. Wu, L. Jiang, L. Wang, Effect of electrochemical modification on the structural characteristics and emulsion storage stability of soy protein isolate, Process Biochem. 75 (2018) 166–172, https://doi.org/10.1016/j.procbio.2018.10.001.

[28] O. Lowry, N. Robert, K. Leiner, M. Wu, A. Farr, Protein measurement with the folin phenol reagent, J. Biol. Chem. 193 (1951) 265–275, https://doi.org/10.1016/S0021-9258(19)52451-6.

[29] D. Li, Y. Zhao, X.u. Wang, H. Tang, N. Wu, F. Wu, D. Yu, W. Elfalleh, Effects of (+)-catechin on a rice bran protein oil-in-water emulsion: Droplet size, zeta-potential, emulsifying properties, and rheological behavior, Food Hydrocolloid. 98 (2020) 105306, https://doi.org/10.1016/j.foodhyd.2019.105306.

[30] C.L. Ladner, R.J. Turner, R.A. Edwards, Development of indole chemistry to label tryptophan residues in protein for determination of tryptophan surface accessibility, Protein Sci. 16 (6) (2007) 1204–1213, https://doi.org/10.1110/ps.062728407.

[31] S. Li, X. Yang, Y. Zhang, H. Ma, Q. Liang, W. Qu, R. He, C. Zhou, G.K. Mahunu, Effects of ultrasound and ultrasound assisted alkaline pretreatments on the enzymolysis and structural characteristics of rice protein, Ultrason. Sonochem. 31 (2016) 20–28, https://doi.org/10.1016/j.ultsonch.2015.11.019.

[32] E. Kristo, A. Hazizaj, M. Corredig, Structural Changes Imposed on Whey Proteins by UV Irradiation in a Continuous UV Light Reactor, J. Agric. Food Chem. 60 (24) (2012) 6204–6209, https://doi.org/10.1021/jf300278k.

[33] Y. Wang, X. Wang, Binding, stability, and antioxidant activity of quercetin with soy protein isolate particles, Food Chem. 188 (2015) 24–29, https://doi.org/10.1016/j.foodchem.2015.04.127.

[34] Y. Sun, S. Zhang, F. Xie, M. Zhong, L. Jiang, B. Qi, Y. Li, Effects of covalent modification with epigallocatechin-3-gallate on oleosin structure and ability to stabilize artificial oil body emulsions, Food Chem. 341 (2021) 128272, https://doi.org/10.1016/j.foodchem.2020.128272.

[35] S. Jiang, J. Ding, J. Andrade, T.M. Rababah, A. Almajwal, M.M. Abulmeaty, H. Feng, Modifying the physicochemical properties of pea protein by pH-shifting and ultrasound combined treatments, Ultrason. Sonochem. 38 (2017) 835–842, https://doi.org/10.1016/j.ultsonch.2017.03.046.

[36] D. Li, X. Li, G. Wu, P. Li, H. Zhang, X. Qi, L.i. Wang, H. Qian, The characterization and stability of the soy protein isolate/1-Octacosanol nanocomplex, Food Chem. 297 (2019) 124766, https://doi.org/10.1016/j.foodchem.2019.05.041.

[37] X. Zhao, F. Chen, W. Xue, L. Lee, FTIR spectra studies on the secondary structures of 7S and 11S globulins from soybean proteins using AOT reverse micellar extraction, Food Hydrocolloid. 22 (4) (2008) 568–575, https://doi.org/10.1016/j.foodhyd.2007.01.019.

[38] Y. Huang, R. Tian, R. Hu, W. Xu, S. Yang, Y. Gong, Expression and Secretion of Functional Recombinant 1 Scu-Pa: Av In Insect Cell Using Signal Peptides, Protein Peptide Lett. 11 (2004) 49–55, https://doi.org/10.2174/0929866043478455.

[39] Z. Zhu, W. Zhu, J. Yi, N. Liu, Y. Cao, J. Lu, E.A. Decker, D.J. McClements, Effects of sonication on the physicochemical and functional properties of walnut protein isolate, Food Res. Int. 106 (2018) 853–861, https://doi.org/10.1016/j.foodres.2018.01.060.

[40] W. Xia, S. Pan, Z. Cheng, Y. Tian, X. Huang, High-Intensity Ultrasound Treatment on Soy Protein after Selectively Proteolyzing Glycinin Component: Physical, Structural, Aggregation Properties, Foods 9 (2020) 839, https://doi.org/10.3390/foods9060839.

[41] Y. Li, Y.u. Cheng, Z. Zhang, Y. Wang, B.K. Mintah, M. Dabbour, H. Jiang, R. He, H. Ma, Modification of rapeseed protein by ultrasound-assisted pH shift treatment: Ultrasonic mode and frequency screening, changes in protein solubility and structural characteristics, Ultrason. Sonochem. 69 (2020) 105240, https://doi.org/10.1016/j.ultsonch.2020.105240.

[42] T.i. Li, X. Li, T. Dai, P. Hu, X. Niu, C. Liu, J. Chen, Binding mechanism and antioxidant capacity of selected phenolic acid-β-casein complexes, Food Res. Int. 129 (2020) 108802, https://doi.org/10.1016/j.foodres.2019.108802.

[43] O.A. Higuera-Barraza, C.L. Del Toro-Sanchez, S. Ruiz-Cruz, E. Márquez-Ríos, Effects of high-energy ultrasound on the functional properties of proteins, Ultrason. Sonochem. 31 (2016) 558–562, https://doi.org/10.1016/j.ultsonch.2016.02.007.

[44] L. Huang, W. Zhang, D. Yan, L. Ma, H. Ma, Solubility and aggregation of soy protein isolate induced by different ionic liquids with the assistance of ultrasound, Int. J. Biol. Macromol. 164 (2020) 2277–2283, https://doi.org/10.1016/j.ijbiomac.2020.08.031.

[45] S.N. Jamdar, V. Rajalakshmi, M.D. Pednekar, F. Juan, V. Yardi, A. Sharma, Influence of degree of hydrolysis on functional properties, antioxidant activity and ACE inhibitory activity of peanut protein hydrolysate, Food Chem. 121 (1) (2010) 178–184, https://doi.org/10.1016/j.foodchem.2009.12.027.

[46] F. Xue, F. Wu, J. Tong, J. Zheng, C. Li, Effect of combination of high-intensity ultrasound treatment and dextran glycosylation on structural and interfacial properties of buckwheat protein isolates, Biosci. Biotech. Bioch. 81 (2017) 1891–1898, https://doi.org/10.1080/09168451.2017.1361805.

[47] X. Pan, Y. Fang, L. Wang, Y. Shi, F. Pei, P. Li, J. Xia, W. Xiong, X. Shen, Q. Hu, M. Xie, Covalent interaction between rice protein hydrolysates and chlorogenic acid: Improving the stability of oil-in-water emulsions, J. Agric. Food Chem. 67 (14) (2019) 4023–4030, https://doi.org/10.1021/acs.jafc.8b06898.